D. Schoellner, S. Lutz, K. Wang, D. Kurtz, T. Kerr, and M. Wang
"A Mechanical-Optical Interface for 25+ Gbps VCSEL/PD Fiber Coupling",
Photonics West Optical Interconnects XVII, SPIE, 10109 (2017).

A Mechanical-Optical Interface for 25+ Gbps VCSEL/PD Fiber Coupling

Dirk Schoellner[a], Sharon Lutz*[a], Ke Wang[a] Dan Kurtz[a], Terrence Kerr[b], Mike Wang[b]
[a]US Conec Ltd., 1138 25th Street SE, Hickory, NC 28602
[b]O-Net Ltd., 756 San Aleso Avenue, Sunnyvale, CA 94085

ABSTRACT

As parallel optics data rates transition from 10 Gbps to 25 Gbps and beyond, VCSELs and photodiodes (PDs) are evolving to support the higher transmission rates. In order to maintain system performance as speeds increase and tolerances become tighter, an improved method is needed to efficiently couple VCSEL/PD array optical outputs to fiber optic networks. The mechanical-optical interface (MOI) is a monolithic component with an array of collimating lenses designed for efficient coupling between the on-board active components and a detachable fiber optic connector.

This paper describes the design and implementation of a next generation MOI to match high speed VCSEL/PD requirements. Improvements to an earlier design were made to accommodate a wider variety of transceiver architectures by taking into account chip driver and wire-bond clearance requirements, while also optimizing the optical design to maximize coupling performance. Monte Carlo simulation results and the sensitivity analysis used to optimize optical performance with respect to VCSEL/PD alignment and coupling requirements are presented.

Empirical testing results are shown to validate the optical model and subsequent system performance; eye-diagram results of a 25 Gbps error-free link are provided across a broad operating temperature range. Environmental and mechanical testing of the component after alignment and adhesion to the circuit substrate validates part and epoxy interaction and performance.

Keywords: VCSEL coupling, mechanical-optical interface, parallel optics, theoretical modeling, 25 Gbps, eye diagrams, fiber coupling, fiber optic connector

1. INTRODUCTION

Progressively faster communications and data processing rates require improvements in the optical links between active optical devices[1]. VCSELs and photo-diodes (PD) are evolving to move from 10 Gbps to 25 Gbps and beyond, and in order to maintain system performance, the designs of critical components must evolve and maintain more stringent part and assembly tolerances. To achieve higher response speeds the PD capacitance must be reduced, necessitating a dramatically reduced available aperture[2]; PD aperture diameters have dropped from approximately 55 microns for 10 Gbps links to less than 35 µm for 25 Gbps links. Optimizing the coupling between the reduced aperture optics and fiber optic connectors is increasingly critical to the performance of the systems[3]. A next generation mechanical-optical interface (MOI) is needed to efficiently couple these faster active VCSEL/PD arrays to fiber optic connectors.

2. BACKGROUND

Coupling between the VCSEL/PD and external fiber optic connectors has previously been achieved through a MOI[4, 5] that was designed for efficient coupling between on-board active components and takes advantage of an existing detachable photonic light-turn (PLT) fiber optic connector[6, 7, 8, 9].

The MOI is a monolithic injection-molded component that is board-mounted above the VCSEL/PD arrays via standard die placement equipment. The next-generation MOI, optimized for high speed applications, shown in Figure 1, contains three features primarily associated with the optical performance of the component and several features for the mechanical alignment between the VCSEL/PD and PLT connector. On the bottom of the MOI, an array of lenses is positioned directly over the VCSEL/PD components and four pedestals control the height between the VCSEL/PD and the lens focal position. Opposite the lens array, on the top of the MOI, there is an optically flat exit window where

collimated light enters and exits the MOI passing between the PLT connector and the active devices. The PLT connector, an injection molded fiber optic connector designed for use with board-level parallel optics, consists of a ferrule that contains the fiber array and has two alignment pins to mate to the MOI. A low-profile housing secures the detachable PLT ferrule to the MOI.

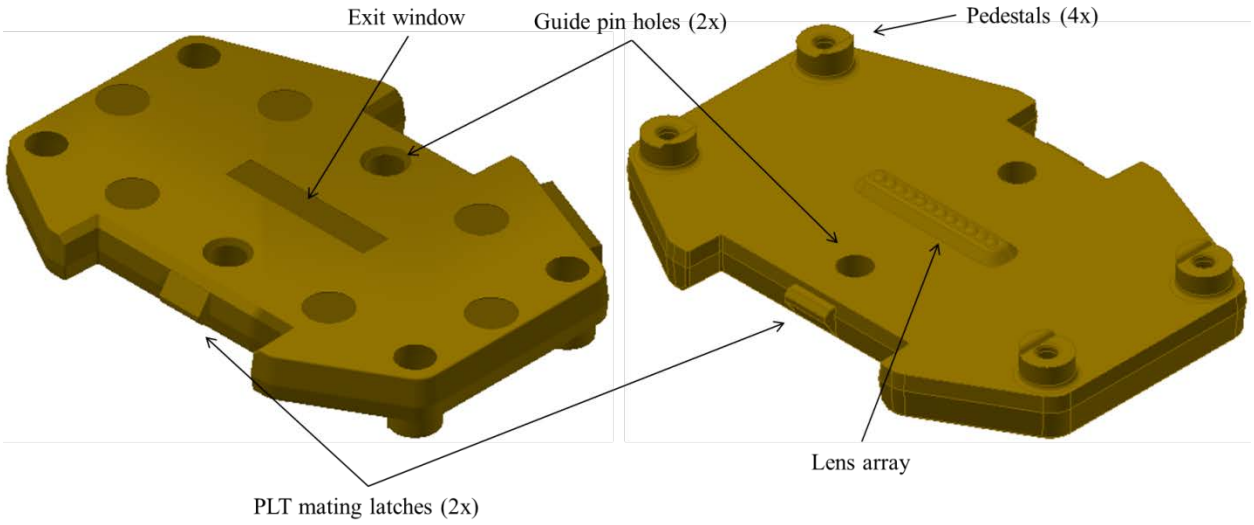

Figure 1. The MOI major features: (left) top side of the MOI, where the PLT ferrule mates using alignment guide pins and (right) bottom side of the MOI, where the lens array is aligned to the VCSEL/PD to capture and couple light.

To simplify precise alignment, the MOI has been designed to be compatible with conventional die bonders. The pedestals, in addition to setting the MOI lens height, also control the epoxy bond-line thickness when the MOI is placed over the VCSEL/PD via the die bonder[4]. Once the MOI has been secured above the VCSEL/PD, the alignment guide holes and latches allow the PLT connector to be snapped into the MOI with micron-level alignment repeatedly and secured with the PLT housing, where the latches secure it in place[10, 11]. The general alignment of the MOI, PLT connector, and housing, as well as the optical path can be seen in Figure 2.

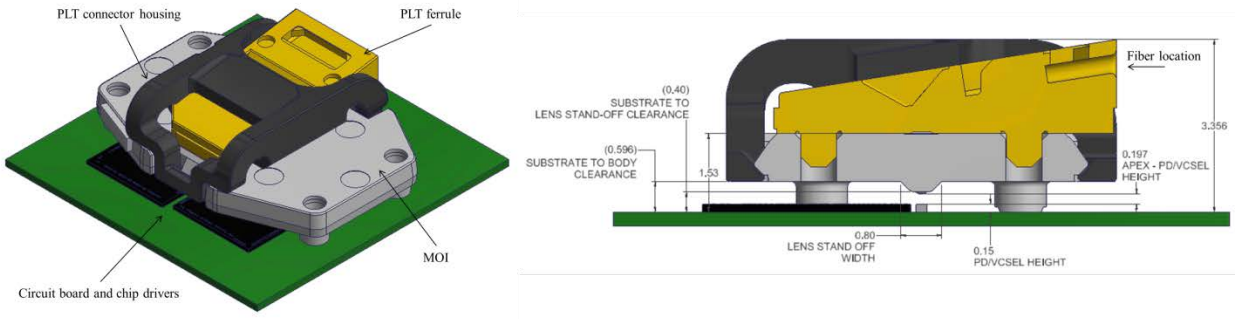

Figure 2. Final assembly configuration of the PLT ferrule secured in place to the MOI with the PLT housing (dimensions in millimeters).

Once the MOI, PLT ferrule, and PLT housing have been combined, an optical path has been created from the VCSEL through to the optical fiber and can easily be coupled to the board edge, off the board, or to other necessary areas. The PLT connector is compatible with both traditional ribbon cable and loose tube round cable jumper assemblies, which are ideal for mid-board routing since round cable jumpers have no preferential bend issues[12].

3. THEORY

The next-generation MOI accommodates a wider variety of transceiver architectures by taking into account the chip driver and wire-bond clearance requirements while optimizing the optical design to maximize coupling performance. MOI design improvements anticipate VCSEL/PD requirements for short-link multi-mode high-speed applications, such as the IEEE 802.3bm 100GBASE-SR4 100m link 100 Gbps standards currently in development[13].

The divergent nature of the VCSEL and fiber emissions lend themselves well to a two lens coupling solution where the first lens, the MOI lens in Tx mode and the total internal reflection (TIR) PLT lens in Rx mode, collimates the beam and the second lens of the system focuses the beam into the fiber core or on to the PD, as shown in Figure 3. This approach also allows the design to be detachable, with the separation being made in the collimated beam space which due to the nature of the expanded beam allows the alignment tolerances between the two lenses to be relatively large.

In order to model and optimize the interface design, a wide range of VCSEL and PD launch/receive conditions were simulated with Zemax. To maintain a cost-effective solution, the MOI lens prescription was designed to accommodate both Tx and Rx components. The single lens prescription limits the optimization routines, but it simplifies production environments related to die bonder programs, test procedures, inventory, and part identification. Despite having larger apertures, the PD coupling and alignment requirements are much more sensitive than VCSEL requirements, and therefore, the optimization process was weighted towards Rx performance. A survey of the common VCSEL and PD dimensions and requirements determined that the space around the optical dies is limited in many applications; wire-bonds, copper traces, and chip drivers vary widely in terms of size, shape, and requirements. Therefore, the MOI was designed to maximize clearance between the MOI lenses and the surface of the VCSEL/PD. In order to capture the light beam and prevent crosstalk between the adjacent channels, the VCSEL launch divergence angle provides a target for the lens location. Using the basic MOI constraints determined by the VCSEL and PD requirements shown in Table 1, optimization was performed to maximize the coupling efficiency while minimizing die bonding alignment requirements. All modeling and charts assume 850 nm light, standard OM3 50/125 µm multi-mode fiber for the PLT connectors, and no anti-reflection (AR) coatings on any of the VCSEL, PD, MOI, or PLT surfaces. AR coatings can mitigate effects of back-reflection, reduce multi-path interference, and improve overall link loss and will be addressed further in section 4.1. In the two following sections, the Tx and Rx modeling results are demonstrated individually followed by the combined link performance in section 3.3. For both Tx and Rx configurations, alignment sensitivity analysis is displayed for individual degrees of freedom using the launch and receive locations shown in Figure 3; the combined effects are also shown as a Monte Carlo analysis in section 3.3.

Table 1. Launch and receive characteristics used for the VCSEL and PD when modeling coupling with the MOI.

Feature	Nominal (µm)	Max (µm)	Min (µm)
VCSEL diameter	7	9	5
VCSEL launch angle	26	32	20
PD diameter	32	55	25

In order to minimize the effect of thermal expansion due to differences between the molded part and the circuit board, the MOI was designed with the lenses located at the center of the attachment pedestals. As the part expands or contracts with temperature, that movement occurs around the center of the lenses, and therefore, movement with respect to the VCSEL/PD is minimized.

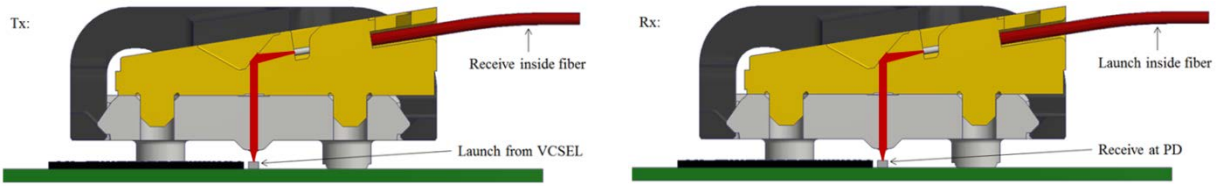

Figure 3. Indication of the launch and detector locations used in modeling the alignment sensitivity and coupling efficiencies of the MOI with respect to the VCSEL/PD.

3.1. Tx Modeling

The Tx performance was modeled to study the light transmission between the VCSEL launch and the receiving fiber located behind the PLT connector. Component misalignment, absorption within the components, and surface reflections were modeled to estimate the coupling losses for the MOI, PLT, and interfaces in between. Figure 4 shows the sensitivity of misaligning the MOI with respect to the VCSEL during die placement for various VCSELs with different divergence angles. Since the PLT connector is attached to the MOI through the guide pin and hole system, the alignment between the MOI and PLT is preserved and assumed to be nominal for the following four figures.

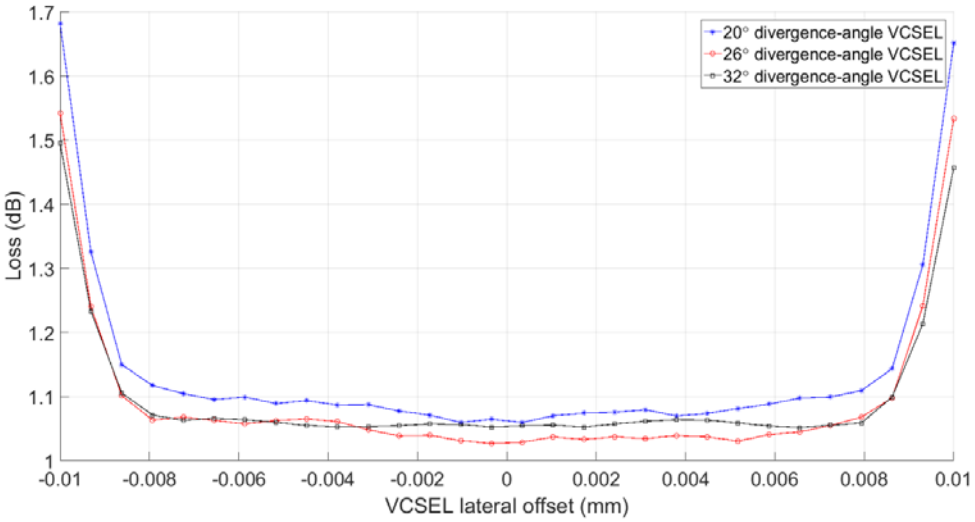

Figure 4. Theoretical lateral offset sensitivity between the MOI and VCSEL for various VCSEL divergence angles.

Figure 5 displays the sensitivity of the same MOI to VCSEL misalignment for VCSELs with different aperture diameters, all with the same 26° divergence angle. For both Figures 4 and 5, as long as the MOI is placed laterally within 8 microns of nominal with respect to the VCSEL, performance will remain at nominal expected values.

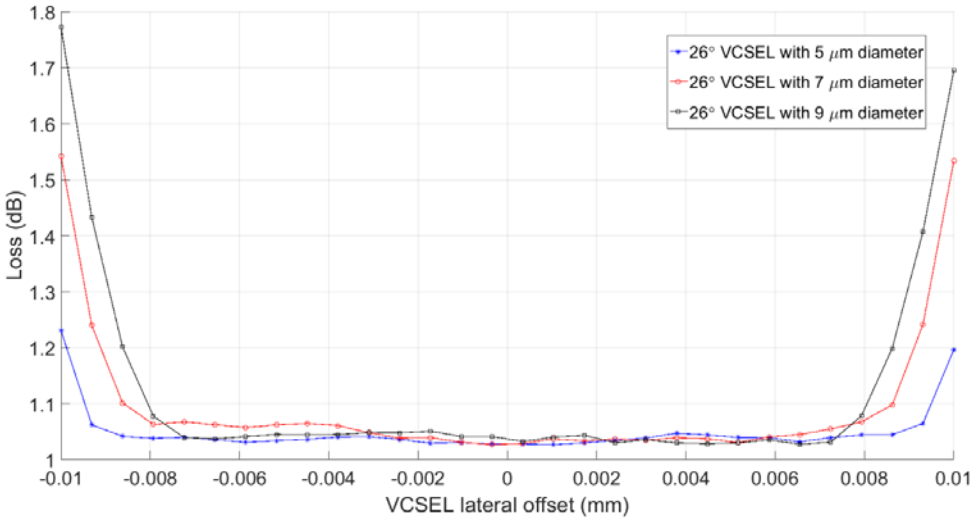

Figure 5. Lateral offset sensitivity for various VCSEL aperture diameters.

Figure 6 displays the vertical alignment sensitivity when placing the MOI over the VCSEL for both the nominal lateral alignment case as well as various combined lateral misalignments. When the MOI is well aligned laterally, a ±20 µm vertical misalignment has very little impact on the performance; therefore epoxy bond-line thickness for both the MOI and VCSEL is not a highly sensitive parameter. However, for larger lateral offsets, such as 6-8 µm, insertion loss does become more sensitive to vertical alignment. Therefore accurate lateral die placement control is critical to repeatable overall performance.

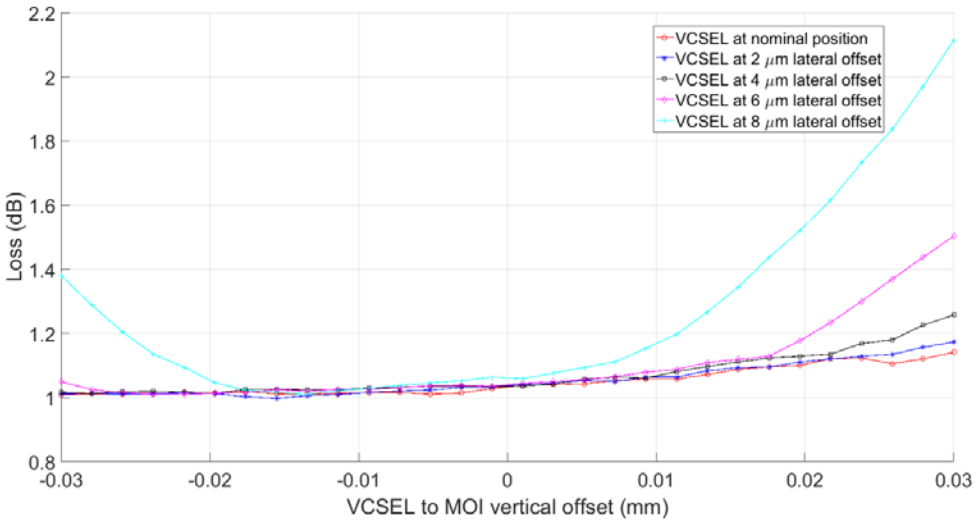

Figure 6. Vertical offset sensitivity for various VCSEL lateral misalignments.

Vertical tilt sensitivity of the MOI with respect to the VCSEL is calculated in Figure 7. Tilt would occur when epoxy bond-lines are not well controlled, and therefore either the VCSEL or MOI is not held parallel to the circuit board. However, due to the small gap between the VCSEL and MOI lenses, insertion loss is very insensitive to tilt of either part. A 3° tilt has no impact on performance, and in a well-controlled die placement process achieving a tilt over 0.5°is highly unlikely.

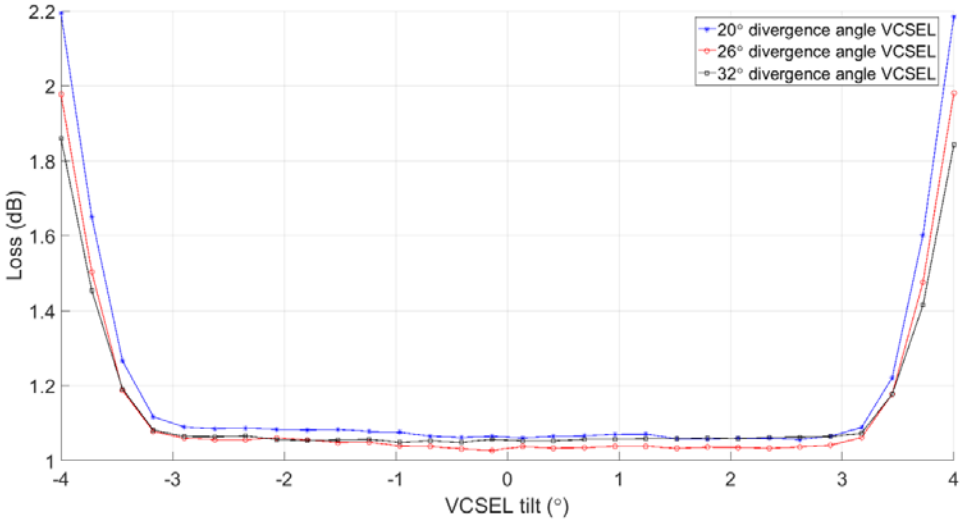

Figure 7. Tilt sensitivity for various VCSEL divergence angles.

3.2. Rx Modeling

Similarly, the Rx performance was modeled to simulate the coupling between the launch fiber and the PD below the MOI lens. Figure 8 shows the sensitivity of lateral misalignment of the PD with various diameters with respect to the MOI. For a nominal 32 µm diameter PD, the MOI needs a lateral placement accuracy of ± 8 µm, but as apertures get smaller, die placement requirements will need to be tightened.

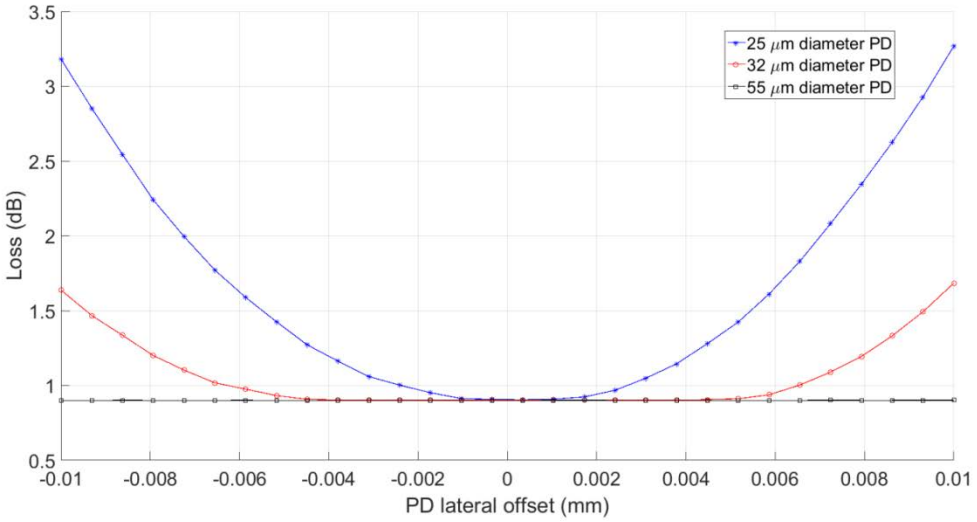

Figure 8. Theoretical lateral offset sensitivity between the MOI and PD for various PD diameters.

Figure 9 displays the vertical offset sensitivity between the MOI and PD surface, as a function of lateral misalignment of the MOI to the PD. When the MOI is correctly aligned laterally, vertical alignment needs to be held to less than ±20 µm of nominal. This vertical alignment includes flatness of the circuit board, epoxy bond line thickness, and accuracy in mating of the two surfaces.

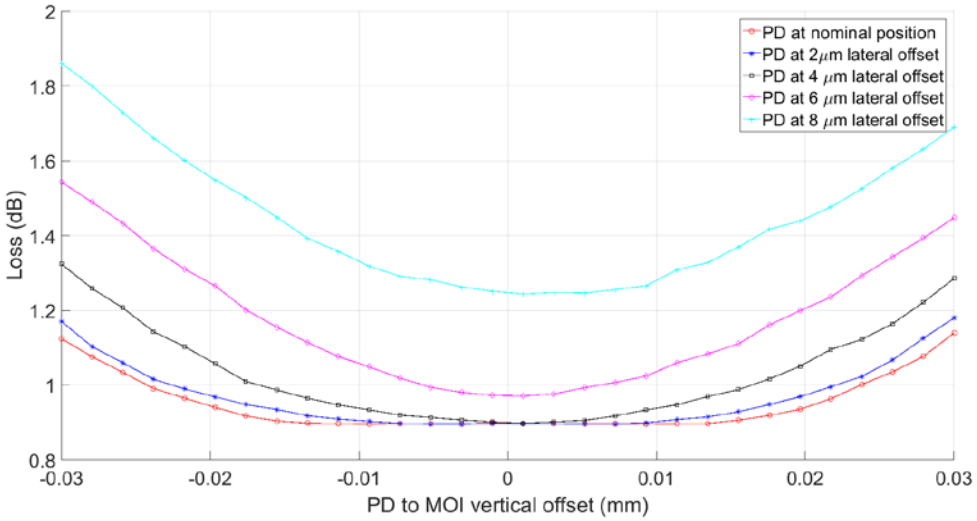

Figure 9. Vertical alignment sensitivity of the PD at different lateral offsets with respect to the MOI.

Figure 10 shows the sensitivity of a tilt between the MOI and PD for various lateral offsets. For a perfect lateral alignment between the MOI and PD, the tilt sensitivity is symmetric regardless of tilt axis. However, with a lateral offset the sensitivity of the tilt becomes more pronounced and decreases the performance of the system.

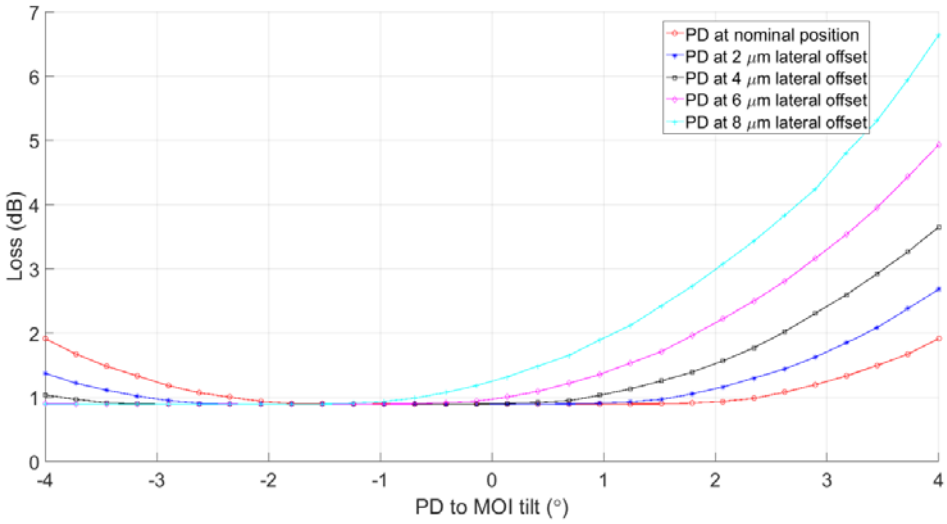

Figure 10. Tilt sensitivity of the PD at different lateral offsets with respect to the MOI.

3.3. Monte Carlo Results

Monte Carlo simulation with 100,000 iterations was run using the parameters from Table 2 to assess total system performance. Figure 11 displays the expected insertion loss performance for a Tx system link, calculated using the change in power from the VCSEL through the PLT connector and coupled into the standard 50 µm multimode fiber. Similarly, Figure 12 displays the expected insertion loss from the fiber, through the PLT connector and MOI, and captured by the PD.

Table 2. Tolerances used for Monte Carlo simulations.

Tolerance Item	Nominal	Min	Max
VCSEL to MOI Lens - Lateral Offset	0 µm	-8 µm	+8 µm
VCSEL to MOI Lens - Distance	200 µm	-13 µm	+13 µm
VCSEL to MOI Lens - Tilt	0 °	- 0.5°	+ 0.5°
VCSEL Beam - Divergence Angle	26°		
VCSEL Aperture Size	7 µm		
PD to MOI Lens - Lateral Offset	0 µm	-8 µm	+8 µm
PD to MOI Lens - Distance	200 µm	-13 µm	+13 µm
PD to MOI Lens - Tilt	0 °	- 0.5°	+ 0.5°
PD Aperture Size	32 µm		

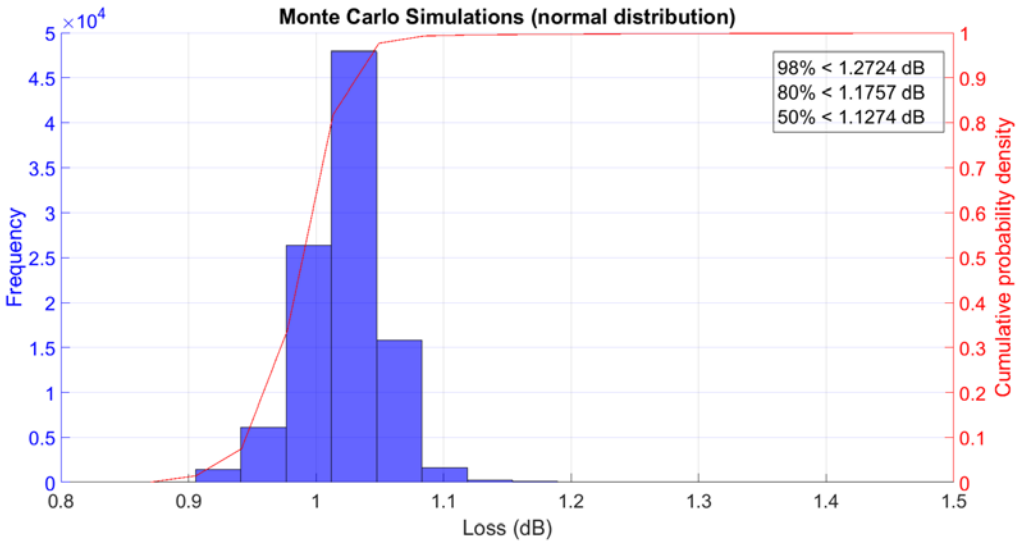

Figure 11. Monte Carlo Tx results using the parameters from Table 2.

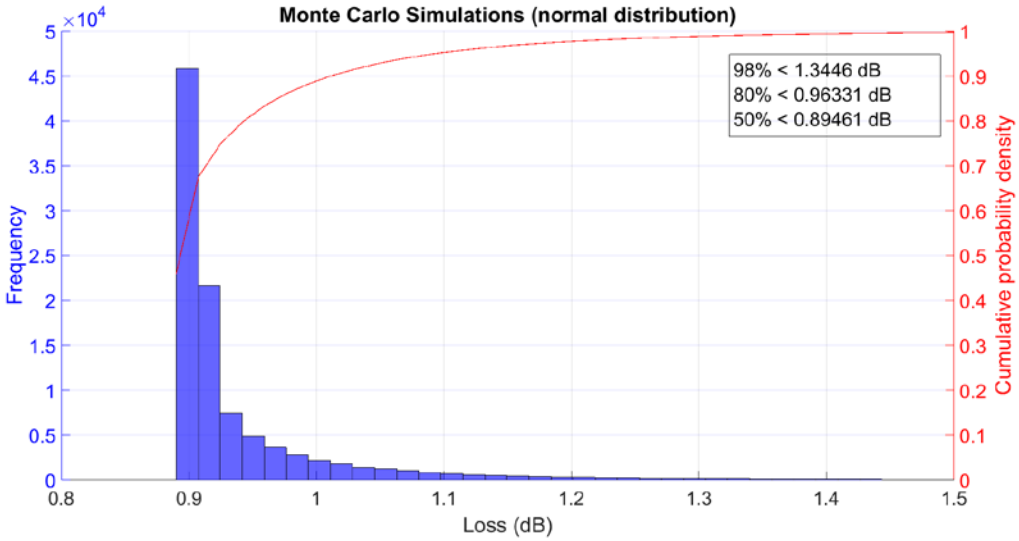

Figure 12. Monte Carlo Rx results using the parameters from Table 2.

Figure 13 displays the full system Monte Carlo simulation results for light launched from a VCSEL through the MOI and coupled into fiber and then back through a MOI to a PD. The fiber was assumed to be lossless and encircled flux conditions maintained within the standard multi-mode fiber.

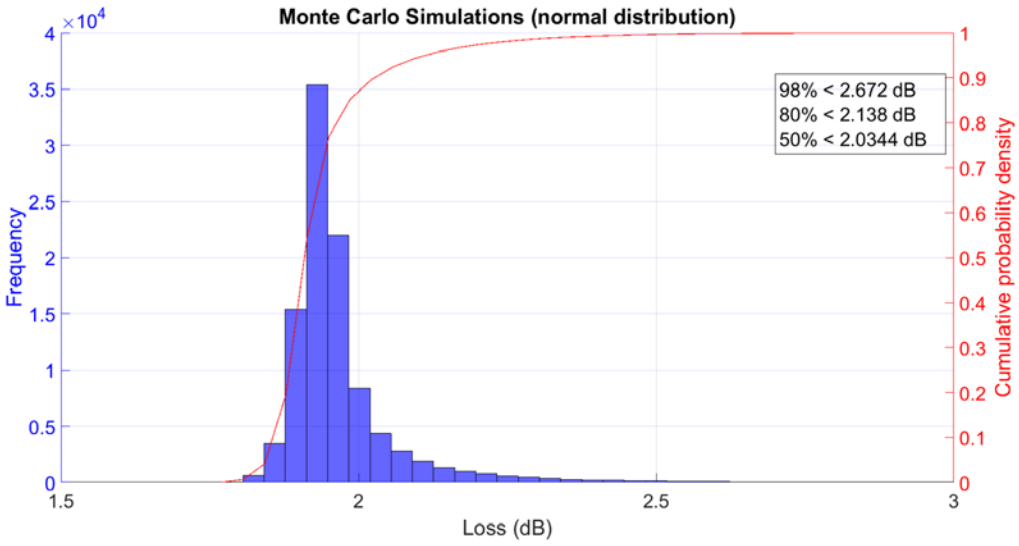

Figure 13. Full system Monte Carlo results using the parameters from Table 2.

3.4. Alignment Considerations

During the design of the transceiver device and circuit board layout, considerations should be made to assist in the development, production and potential troubleshooting of the finished product. All of the sensitivity plots in the above figures are for a single VCSEL/PD position with respect to a single MOI lens. As the final device will have parallel active devices aligned to multiple lenses, care must be taken to ensure suitable alignment of each channel is possible. VCSELs and PDs are generally used in arrays, for example, a block of four VCSELs will be placed adjacent to a block of four PDs for use with one MOI. Therefore, the placement of one device block with respect to the other has an impact on the overall achievable alignment and uniformity of channel performance. In order to achieve the performance indicated by the Monte Carlo simulations above, the alignment between each lens and the active device must be less than 8 µm; if the PD array can only be placed ±2 µm to the VCSEL array, as illustrated in Figure 14 below, then 2 µm of the MOI lateral alignment tolerance has already been consumed. This VCSEL to PD alignment effect, along with the other tolerances involved, may make active optical alignment of the MOI desirable for optimal system performance in some cases. As the PLT connector is easily detachable, the MOI is designed to be suitable for active alignment with respect to both the VCSELs and PDs via a loopback connection at the end of the PLT connection.

In order to study and understand alignment tolerances for specific applications, it may be desirable to measure the alignment between a MOI and VCSEL/PD after assembly. A set of fiducial features that can be seen after attachment of the MOI is a desirable feature which can be useful in several scenarios, as shown in Figure 14. These can be used during product development to study the stability of the attachment or for troubleshooting performance issues by measuring, for example, from the fiducial mark to the MOI guide holes and from the fiducial mark to VCSEL/PD arrays when the MOI is removed or prior to attachment. Including fiducial marks in the design of the circuit board and controlling the placement of the active arrays with respect to them could also allow, with proper development of the process, measurement of the lens outline through the MOI exit window with respect to these fiducials. Although a properly selected imaging metrology solution is a viable technique for verifying alignment, imaging through the MOI to the VCSEL/PD is not a suitable method. Since the MOI lenses are designed to be collimating and not imaging lenses, optical imaging through the lenses is neither an accurate or viable measurement technique.

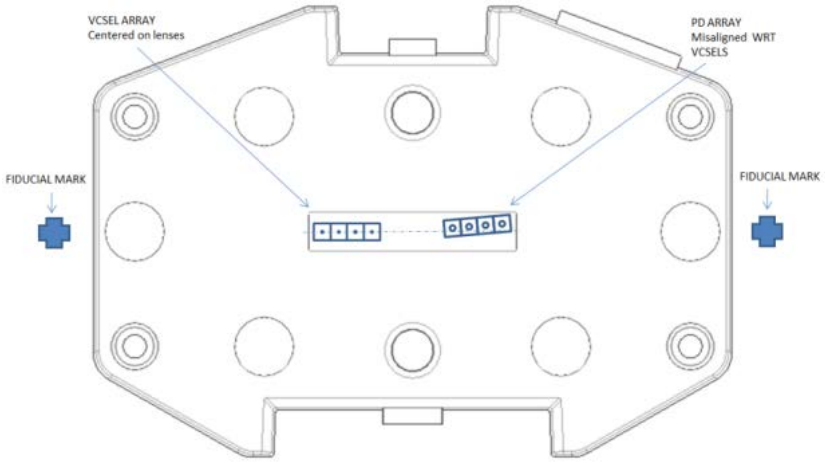

Figure 14. Illustration to show the effect of VCSEL to PD alignment on the overall alignment of each to the MOI lenses. Also shown are conceptual fiducial marks on the circuit board that can be used for subsequent development and production verification.

4. EMPIRICAL PERFORMANCE

4.1. Insertion Loss and Transmission

Empirical testing was conducted to validate the developed theoretical model. To establish a transmission baseline, a standard insertion loss test system was used to measure the absorption and return reflection through a PLT and MOI Rx link, independent of VCSEL or PD performance. The insertion loss launch cable, terminated with a standard MTP connector, was referenced to negate system losses and reflections, and then a PLT connector was attached and insertion loss was measured. The average PLT connection loss was 0.3 dB, primarily due to absorption within the optical path in the connector and a return reflection from the part to the air at the exit window. A MOI was then attached and the insertion loss remeasured; the average additional loss was 0.6 dB, primarily due to the front surface reflection of the MOI exit window as the light enters the part. It is important to note that since there is an MTP glass-to-air reflection in the reference path but physical contact eliminates that reflection during subsequent measurements once the PLT connector has been added, impacting the measurement by 0.15 dB[14]. That 0.15 dB reflection loss must be added back into the 0.30 dB PLT measurement to compensate for the unreferenced reflection interface, and therefore the total PLT insertion loss is 0.45 dB. Summing the performance of the PLT and MOI components, the measured link loss is 1.05 dB. This result is comparable to the theoretical calculation in Figure 8, which predicts a nominal loss of 0.9 dB. The loss constitutes both the reflection and absorption losses of the PLT connector and the MOI. Approximately half of the total loss is caused by reflections at the two exit windows. If it is necessary for specific applications, anti-reflection (AR) coatings can be applied to the exit window of either the PLT or the MOI connector to mitigate the surface reflections. While there is an additional cost to such component processing, adding an AR coating to both exit windows would eliminate half of the system loss calculated above and would reduce the insertion loss displayed in all of the theoretical loss curves of section 3 by half as well.

4.2. Adhesion

The MOI is attached to the circuit board during the die placement process using a UV-curable epoxy in order to lock the part in place while minimizing movement. Multiple epoxies have been studied in order to identify a suitable epoxy that adheres to both the MOI and the FR4 circuit board while minimizing epoxy shrink and part movement. Depending on the application, a single UV-curable epoxy may be sufficient for the final part adhesion. In cases where stronger bond is needed, a secondary thermal epoxy can be added around the pedestals in order to reinforce the epoxy performance after the UV cure is complete. Epoxies for both the UV-cure and secondary thermal process have been identified and tested through a stringent environmental qualification procedure. MOI components were placed on the circuit boards and epoxied in place in two groups, one with only the UV epoxy, and the other with both the UV and secondary thermal cure

epoxy. MOIs were attached to the circuit board using UV-curable epoxy NextGen AB36-HV and were cured with a 365 nm LED at 300 mW/cm^2 for 60 seconds. Half of the parts were then reinforced with a thermal cure epoxy, Fiber Optic Center AB9320, which was cured at 85°C for 55 minutes. A baseline group of both sets of parts was tested using a force gauge to establish the epoxy failure point in both tensile and sheer applications. Tensile testing consisted of applying a force directly to the MOI through a hole in the circuit board while monitoring the force versus displacement curve to determine the epoxy failure point, as shown in Figure 16 (center). Sheer testing followed a similar test regime, but with the force applied to the side of the MOI, as indicated in Figure 16 (right). Tensile testing simulates the insertion or removal of the PLT connector; a PLT housing is designed to release under 5 N to 9 N of applied force. Sheer testing simulates stress applied to the MOI via the stiffness of the fiber and cable routing. After baseline testing, the remaining parts were placed in a thermal oven for a series seven day trials at each temperature/humidity profile shown in Table 3.

Figure 15. (Left) Setup used in testing the MOI adhesion to the circuit board. (Center) Tensile test to simulate stress during the PLT connector insertion and removal. (Right) Sheer test to simulate force applied by fiber routing of the cables associated with the PLT connector.

Table 3. Environmental conditions components were subjected to serially while qualifying epoxy adhesion performance.

Temperature / Humidity	**Days**
85°C / 85%RH	7 days
-40°C to 75°C cycling every 60 minutes	7 days
95°C / 95%RH	7 days
110°C	7 days

After the second step, half of the parts were tested to failure for sheer and tensile data and the remaining components were tested after completion of the full four step test regime; Table 4 shows the results of tensile and sheer testing for both the UV and UV/thermal epoxies after all four test steps. After 28 days of environmental exposure, the minimum results shown in Table 4 still surpass the PLT mating forces with a significant safety margin.

Table 4. Average and worst-case results for MOI adhesion for both the baseline performance and after environmental testing (all units are in Newtons). Post-environmental results contain test results after both the 14th and 28th day and minimum value is inclusive of all test data.

Epoxy	Test	Average		Minimum	
		Baseline	Post-Env	Baseline	Post-Env
AB14-UV	Shear	77.3	43.8	71.3	25.6
	Tensile	58.6	36.8	49.6	16.4
AB14-UV and AB9320	Shear	95.1	64.8	76.6	47.1
	Tensile	69.6	59.6	47.3	46.5

5. EXPERIMENTAL RESULTS

In order to establish link performance, 25 Gbps active optical cables (AOC) were build using the MOI and PLT components. The AOCs were ramped from 0°C to 70°C while running at 25.78 Gbps per channel. All four channels are displayed in Figure 17; the first row is operating at 0°C, the second row is at room temperature, and the final row is at 70°C. Despite the wide temperature range, signal integrity remained stable. During a seven minute run, the signal remained error free.

Figure 16. A four channel AOC running at 25 Gbps using the MOI and PLT connector for coupling. The AOC was cycled from 0°C to 70°C (rows 1 to 3, respectively) and showed no degradation in performance.

6. SUMMARY

As applications continue to develop for mid-board optical interconnects, a new mechanical-optical interface has been developed to efficiently couple high-speed VCSEL/PDs to fiber optic networks. Zemax modeling and Monte Carlo simulations were used optimize optical performance, and sensitivity analysis indicates that component alignment and

placement using conventional die bonders is readily achievable. Eye diagrams from fully functional 25 Gbps per channel AOCs were presented, including a seven minute error free run across all four channels.

Future development of the MOI component may include support for higher channel counts since the IEEE 802.3bs working group has recently standardized 16 channel lane counts for 400 Gbps applications[15]. Additional increases in data rates will continue to reduce PD aperture sizes and VCSEL beam outputs will also further diverge. These active optics changes may involve a new lens prescription to support even smaller spot diameter requirements. With the continued development of single-mode VCSEL and PD apertures, a new lens prescription may support coupling for single-mode fiber applications, although the alignment sensitivity may present challenges with existing passive placement capabilities and necessitate active alignment.

REFERENCES

[1] Dove, D., Shrikhande, K., Anslow, P., King, J. and Latchman, R., "IEEE 802.3 Next Generation 100 Gb/s Optical Ethernet Call-For-Interest Consensus," IEEE 802.3, San Francisco, (2011).

[2] Agrawal, G. P. , [Lightwave Technology: Components and Devices], Wiley, (2004).

[3] Ugolini, A., Childers, E., Hastings, D., Schoellner, D. and Wakjira, J., "Performance Characterization of a Modular Miniature Photonic Turn Connector and Optical Module Interface," Proceedings of the International Wire & Cable Symposium, (2010).

[4] Chuang, S., Schoellner, D., Wakjira, J., Ugolini, A. and G. Wolf, "Development and Qualification of a Mechanical-Optical Interface for Parallel Optics Links," Photonics West Optical Interconnects XV Proc. SPIE 9368, (2015).

[5] Chuang, S., Schoellner, D., Ugolini, A., Wakjira, J., Wolf, W., Gandhi, P. and Persaud A., "Theoretical and Empirical Qualification of a Mechanical-Optical Interface for Parallel Optics Links," Photonics West Optical Interconnects XV Proc. SPIE 9368, (2015).

[6] Childers, D., Childers, E., Graham, J., Hughes, M., Schoellner, D. and Ugolini, A., "Miniature Detachable Photonic Turn Connector for Optical Module Interface," IEEE Electronic Components and Technology Conference, (2011).

[7] Benner, A., Kuchta, D., Pepeljugoski, P., Budd, R., Hougham, G., Fasano, B., Marston, K., Bagheri, H., Seminaro, E., Xu,H., Meadowcroft, D., Fields, M., McColloch, L., Robinson, M., Miller, F., Kaneshiro, R., Granger, R., Childers, D. and Childers, E., "Optics for High-Performance Servers and Supercomputers," OFC 2010: Beyond Telecom and Datacom Symposium III, (2010).

[8] Kuchta, D., Rylyakov, A., Schow, C., Proesel, J., Baks, C., Westbergh, P., Gustavsson, J. and Larsson, A., "64Gb/s Transmission over 57m MMF using an NRZ Modulated 850nm VCSEL," OFC 2014: Low Power VCSEL Interconnect, (2014).

[9] Iles, G., Jones, J. and Rosea, A., "Experience Powering Xilinx Virtex-7 FPGAs," Topical Workshop on Electronics for Particle Physics, (2013).

[10] Childers, D., Childers, E., Graham, J., Hughes, M., Schoellner, D. and Ugolini, A., "Miniature Detachable Photonic Turn Connector for Parallel Optic Transceiver Interface," Optical Fiber Communication Conference and Exposition and the National Fiber Optic Engineers Conference, (2011).

[11] Childers, E., Hastings, D., Schoellner, D., Ugolini, A. and Wakjira, J., "Performance Methodologies of a Modular Miniature Photonic Turn Connector," Photonics West SPIE 8630 Optoelectronic Interconnects XIII, (2013).

[12] Smith, T. and Bishop, G., "Ribbon vs. Loose Tube Fiber Cabling," Optical Fiber Communication Conference and Exposition and the National Fiber Optic Engineers Conference, (2006).

[13] Juniper, "100-Gigabit Ethernet 100GBASE-R Optical Interface Specifications," 21 June 2016, <https://www.juniper.net/documentation/en_US/release-independent/junos/topics/reference/specifications/transceiver-m-mx-t-series-100gebase-optical-specifications.html#jd0e114> (8 December 2016).

[14] Schoellner, D., Wakjira, J., Chuang, S. and Lutz, S., "Performance Methodology and Characterization of a Multi-Fiber Expanded Beam Lensed Optical Interconnect," IEEE Electronic Components and Technology Conference, (2016).

[15] Kolesar, P., Lingle, R. and Ugolini, A., "400GBASE-SR16 Cabling," September 2014, <http://www.ieee802.org/3/400GSG/email/pdf2XrN5gMdmE.pdf> (15 December 2016).